JOURNAL OF SPACECRAFT AND ROCKETS
Vol. 41, No. 3, May–June 2004

Numerical Simulation of Rolling Airframes Using a Multilevel Cartesian Method

Scott M. Murman*
ELORET, Moffett Field, California 94035
Michael J. Aftosmis†
NASA Ames Research Center, Moffett Field, California 94035
and
Marsha J. Berger‡
Courant Institute, New York, New York 10012

A supersonic rolling missile with two synchronous canard control surfaces is analyzed using an automated, inviscid, Cartesian method. Sequential-static and time-dependent dynamic simulations of the complete motion are computed for canard dither schedules for level flight, pitch, and yaw maneuvers. The dynamic simulations are compared directly against both high-resolution viscous simulations and relevant experimental data and are also utilized to compute dynamic stability derivatives. The results show that both the body roll rate and canard dither motion influence the roll-averaged forces and moments on the body. At the relatively low roll rates analyzed in the current work these dynamic effects are modest; however, the dynamic computations are effective in predicting the dynamic stability derivatives, which can be significant for highly maneuverable missiles.

Nomenclature

C_A	=	axial force coefficient
C_l	=	rolling moment coefficient
C_m	=	pitching moment coefficient
C_N	=	normal force coefficient
C_n	=	yawing moment coefficient
C_Y	=	lateral force coefficient
c	=	speed of sound
e	=	internal energy
$\boldsymbol{f}$	=	Euler flux vector
g	=	magnitude of gravitational acceleration
L	=	length, reference length = base diameter
M	=	Mach number
$\boldsymbol{n}$	=	normal direction vector
p	=	pressure, or roll rate in Sec. III.C
$\boldsymbol{Q}$	=	conserved mass, momentum, and energy vectors
S	=	area, reference area = base area
Sr	=	Strouhal number, fD/V_∞
t	=	time
$\boldsymbol{u}$	=	velocity vector
V	=	volume
V_∞	=	freestream velocity
α	=	angle of attack, deg
δ	=	canard pitch angle
ρ	=	density
τ	=	pseudotime
ϕ	=	body roll angle, deg
$\dot{\phi}$	=	body roll rate, Hz

Subscripts

c	=	canard
D	=	body diameter
n	=	normal direction
∞	=	freestream
Ω	=	computational domain

Superscript

$n, n+1$	=	discrete time level

I. Introduction

THE use of computational fluid dynamics (CFD) to simulate steady flow about static geometries is now common practice for engineers and analysts. The ability to routinely simulate dynamic configurations, where the geometry moves in some manner during a computation, however, is still a computationally intensive problem. For many applications, such as rotorcraft, turbines, or rolling missiles, the motion of the body is a fundamental aspect of the simulation and must be accounted for in some manner. The current work demonstrates an inviscid Cartesian method for simulating a rolling airframe with movable canard control surfaces. The Cartesian method provides an efficient, automated, and robust approach for performing CFD simulations about arbitrarily complex geometries.[1,2]

There are several numerical schemes capable of simulating a dynamic configuration where active control surfaces move relative to the body[3–6]; however, few methods have been applied to the analysis of a rolling airframe. Weinacht et al.[7,8] demonstrated methods for analyzing axisymmetric geometries using steady-state algorithms to determine the pitch-damping coefficient. Recently, Oktay and Akay[9] and Park et al.[10] performed unsteady dynamic simulations of a simple finned missile geometry using rigid domain motions to compute a general set of dynamic stability derivatives. Janus et al.[11] demonstrated a multiblock structured approach for relative body motion on a prop-fan cruise missile, and recently Hall[12] applied an overset structured approach to the simulation of a rolling airframe with dithering canards.

The current work presents a general Cartesian method for simulating moving geometries with relative body motion in three-dimensions. The use of a Cartesian scheme allows these dynamic simulations to be carried out in an automated manner. This method

Received 20 August 2002; revision received 9 June 2003; accepted for publication 11 June 2003.

*Senior Research Scientist; smurman@nas.nasa.gov. Member AIAA.
†Research Scientist, NASA Advanced Supercomputing Division. Senior Member AIAA.
‡Professor, Computer Science Department. Member AIAA.

is applied to the simulation of a rolling missile with both fixed and moving canard control surfaces. An efficient scheme for computing dynamic stability derivatives using rigid domain motions is presented and utilized to compute the damping coefficients for the current missile configuration. Comparisons are made for the current results between static and dynamic simulations, against high-fidelity viscous simulations,[13] and also against relevant experimental data.[14]

II. Numerical Method

A. Geometry and Computational Mesh

The canard-controlled missile considered in this work is shown in Fig. 1 for its zero-roll ($\phi = 0$ deg) configuration. The canards are shown in their zero-deflection position. The body is approximately shaped like a hemisphere cylinder and has a fineness ratio (length/diameter) of roughly 20. The center of gravity (moment center) for the current configuration is located a half body length from the nose. There are four fixed, interdigitated tails, which are canted 1 deg to generate a counterclockwise roll when viewed from the nose, and two canards that act as control surfaces. These canards are interconnected so that their motion is synchronous, and as the body rolls the canards can change positions to affect controlled movements such as yaw or pitch. This canard motion is sometimes referred to as "dithering." Two canard dither schedules based on an analytic model of the actual flight guidance system are considered in this work. Both dither schedules are outlined in Fig. 2 for a body roll rate of 8.75 Hz (positive roll is counterclockwise when viewed from the nose). The canards can sustain only two positions: either the minimum or maximum deflection angle, which is ± 15 deg in this case. As the body rolls, the canards dither between their minimum and maximum deflection angles at discrete roll positions. For example, in dither schedule 0 the canards start to move from -15 deg deflection at $\phi = 0$ deg. The time of travel between the two deflection angles corresponds to approximately 21 deg of roll at this roll rate, so that at $\phi = 21$ deg the canards are positioned at $+15$ deg deflection. It is also possible that the canards do not complete their travel before being instructed to "reverse," as can be seen in Dither Schedule 1 near $\phi = 200$ deg. Both of the canard dither schedules are periodic over one complete revolution of the body.

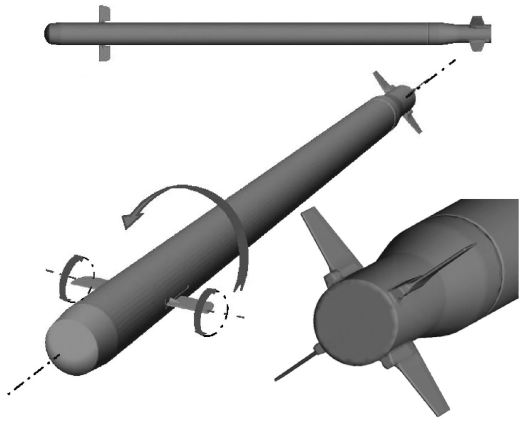

Fig. 1 Canard-controlled missile surface geometry.

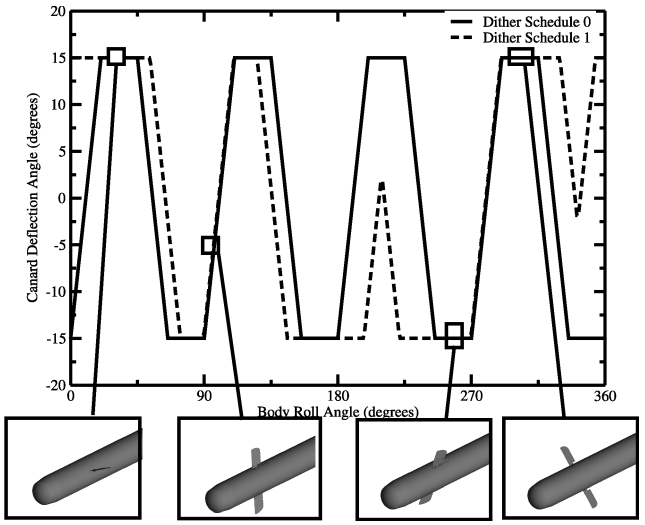

Fig. 2 Motion of canard control surfaces for 8.75-Hz body roll rate. The canards can sustain only two positions: either the minimum or maximum deflection angle, which is ± 15 deg in this case.

The current configuration poses a challenge, especially when creating a computational mesh on which one can compute a solution efficiently, due to the large variation in physical scales that must be resolved. The sharp edges of the canards must be resolved to generate strong canard tip vortices. These canard vortices must be preserved as they convect the length of the body in order to resolve the canard vortex–tail interaction that occurs at low-to-moderate angles of attack. Furthermore, the large bow shock that forms ahead of the body in supersonic flow, as well as the shock structures around the canards and fins, must also be resolved. Volume mesh generation was performed using the Cartesian meshing scheme of Aftosmis et al.[1] This package takes as input the triangulated surface geometry and generates an unstructured Cartesian volume mesh by subdividing the computational domain based on the geometry. In this manner, the sharp geometric features contain refined cells while areas away from the geometry maintain a relatively coarse spacing. The intersection of the solid geometry with the the regular Cartesian hexahedra is computed, and polyhedral cells are formed that contain the embedded boundary. Cells in regions interior to the solid geometry are removed. The solid-wall boundary conditions for the flow solver are then specified within these "cut-cell" polyhedra. The volume meshing procedure is robust and does not require user intervention. (See Refs. 1 and 15 for more details on Cartesian volume meshing.) Optionally, volume regions within the domain can be specified to contain a specific resolution. These prespecified regions are utilized in the current work to resolve the bow shock ahead of the body and the canard vortex trajectory on the leeward side of the fuselage. Fig. 3 shows a lateral cutting plane through the canard, as well as two axial cutting planes along the body: one just behind the canards, and one intersecting the tail section. The resolved regions for the shocks and the uniform vortex region the length of the body are clearly visible, as well as the refinement near the sharp features of the geometry such as the leading and trailing edges of the canards and the tips of the tail fins.

A grid-resolution study was performed using a static missile configuration at flow conditions $M_\infty = 1.6, \alpha = 3.0$ deg, and $\phi = 0.0$ deg and with the canards undeflected. These flow conditions represent a nominal baseline configuration for the current work, whereas the undeflected canards still generate strong vortices that impact the tail section. Simulations were performed using three mesh densities: 1.2×10^6, 3.4×10^6, and 6.0×10^6 cells. Computed results were compared in terms of the axial and normal forces and pitching and rolling moments on the body. The difference between the medium and finest grids in terms of the integrated quantities was less than 3%. Comparison with highly refined viscous simulations[13] also showed results consistent with the difference between inviscid and viscous simulations. Based on these findings, a grid density of roughly 3.4×10^6 cells was utilized for all of the simulations, and this is the level of refinement shown in Fig. 3.

B. Cartesian Moving-Body Flow Solver

To simulate a rolling missile with dithering canards, a scheme is needed that allows rigid bodies to move relative to each other during a simulation. A general numerical scheme for solving time-dependent flows with (optional) rigid-body motion for unstructured Cartesian meshes was developed from the parallel, steady-state solver of Aftosmis et al.[2] This section provides a brief overview of the scheme. Further details and analysis of the numerical scheme are provided in Ref. 16.

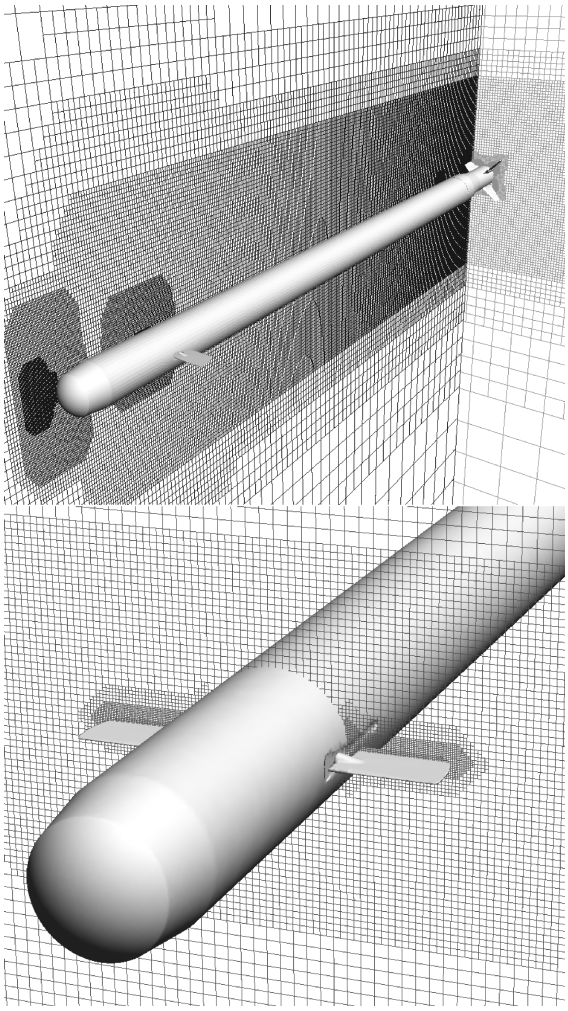

Fig. 3 Cutting planes through Cartesian mesh.

1. Dual-Time Formulation

To leverage the infrastructure of the steady-state flow solver outlined in Ref. 2, a dual-time formulation[17,18] was developed for the following time-dependent scheme:

$$\frac{\mathrm{d}\boldsymbol{Q}}{\mathrm{d}\tau} + R^*(\boldsymbol{Q}) = 0$$

$$R^*(\boldsymbol{Q}) = \frac{\partial \boldsymbol{Q}}{\partial t} + R(\boldsymbol{Q}) \tag{1}$$

where τ is referred to here as "pseudo-time" and is the iterative parameter, t is the physical time, $\boldsymbol{Q}$ is the vector of conserved variables, and $R(\boldsymbol{Q})$ is an appropriate numerical quadrature of the flux divergence, $1/V \oint_S \boldsymbol{f} \cdot \boldsymbol{n} \mathrm{d}S$. As $\mathrm{d}\boldsymbol{Q}/\mathrm{d}\tau \to 0$ the time-dependent formulation is recovered. The multigrid solver described in Ref. 2 is used to efficiently converge the inner pseudo-time integration. An explicit, multistage, pseudo-time-integration scheme is utilized to converge the "inner loop" in Eq. (1). This is similar to the scheme outlined by Jameson[19]; however, the semi-implicit approach of Melson et al.[20] is used here for the physical time-derivative term.

Various time-dependent schemes can be constructed for Eq. (1) by appropriately discretizing the time derivative. In the current work, it is desirable to use an unconditionally stable, implicit scheme to allow a large time step to be chosen based on physical considerations rather than a potentially smaller stability-limited time step. In the Cartesian embedded-boundary scheme, the cut-cell polyhedra can have arbitrarily small volumes, and a stability limit can be very restrictive. Using a large time step also reduces the amount of computational work required to process the moving geometry and mesh through a complete simulation. In the current work, the backward Euler and second-order backward time-integration schemes have both been utilized.

2. Arbitrary Lagrangian–Eulerian Formulation

Considering the motion of the rolling missile with dithering canards described in Sec. II.A in a body-fixed frame, the regions where relative motion occur are confined to a small area surrounding the canards. This is not unique to rotating airframes and occurs in many applications such as rotorcraft or stage separation from space vehicles. It is desirable to simulate the rotation of the entire missile using a rigid-body motion of the entire computational domain and to treat the relative motion of the canards separately within the rotating domain. This approach limits the amount of computational work that is required to process the moving geometry.

An arbitrary Lagrangian–Eulerian (ALE) formulation is utilized to account for the rigid-body motion of the computational domain. (See Ref. 21 for the development of the ALE formulation.) This is accomplished by modifying the flux through a boundary to account for the motion of the boundary. For the inviscid flux vector utilized here, this becomes

$$\boldsymbol{f} \cdot \boldsymbol{n} = \begin{Bmatrix} \rho u_n \\ \rho u_n \boldsymbol{u} + p\boldsymbol{n} \\ \rho u_n e + p\boldsymbol{u} \cdot \boldsymbol{n} \end{Bmatrix} \tag{2}$$

where

$$u_n = (\boldsymbol{u} - \boldsymbol{u}_\Omega) \cdot \boldsymbol{n}$$

is the velocity relative to the moving boundary and $\boldsymbol{u}_\Omega$ is the velocity of the moving domain. Hence, the convective part of the flux is modified to account for the motion of the boundary, compared to the treatment for a fixed domain. A modified form of van Leer's flux-vector splitting[22] is used with the ALE formulation. This modification uses the Mach number relative to the moving boundary, $M_n c = (\boldsymbol{u} - \boldsymbol{u}_\Omega) \cdot \boldsymbol{n}$, when determining the characteristic speeds of the system.

3. Relative motion

Figure 4 shows a schematic of a rigid body moving through a fixed Cartesian mesh over one discrete time step. The shaded region highlights cells that have been "swept" by the body through the time step. These swept cells change volume and shape over the time step and can appear or disappear (or both) as well. This section briefly describes a scheme for optionally including such relative motion within a moving rigid domain. The equations of motion for the deforming cells can be written in an integral conservation form as

$$\int_{V(t)} \boldsymbol{Q} \mathrm{d}V = \left[- \oint_{S(t)} \boldsymbol{f} \cdot \boldsymbol{n} \mathrm{d}S \right] \mathrm{d}t \tag{3}$$

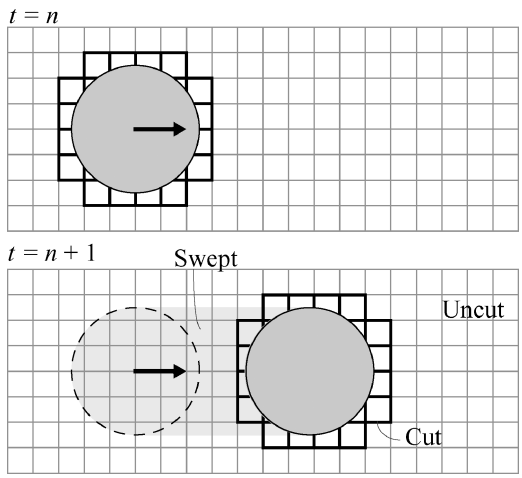

Fig. 4 Schematic of a rigid body moving through a Cartesian mesh.

Integrating Eq. (3) using the backward Euler scheme gives

$$\frac{\boldsymbol{Q}^{n+1} - (V^n/V^{n+1})\boldsymbol{Q}^n}{\Delta t} = -\frac{1}{V^{n+1}}\left[\sum \tilde{f}\cdot \boldsymbol{n}\Delta S\right]^{n+1} \tag{4}$$

This can be numerically integrated using the dual-time scheme outlined earlier. The term $(V^n/V^{n+1})\boldsymbol{Q}^n$ becomes a fixed source term in the dual-time scheme. However, $\boldsymbol{Q}^n$ is only available on the mesh at time level n, while it is required on the mesh at time level $n+1$ in order to integrate Eq. (4). Rewriting Eq. (4) gives

$$\frac{\boldsymbol{Q}^{n+1} - \hat{\boldsymbol{Q}}^n}{\Delta t} = -\frac{1}{V^{n+1}}\left[\sum \tilde{f}\cdot \boldsymbol{n}\Delta S\right]^{n+1} \tag{5}$$

where $\hat{\boldsymbol{Q}}^n$ represents the state vector at time level n on the mesh at time level $n+1$.

In the current scheme, the vector $\boldsymbol{Q}^n$ is "mapped" from the mesh at time level n to the new mesh at $n+1$ using an interpolation operator I_n^{n+1}:

$$\hat{\boldsymbol{Q}}^n = I_n^{n+1}\boldsymbol{Q}^n \tag{6}$$

If $I_n^{n+1} = V^n/V^{n+1}$ then Eq. (4) is satisfied. The interpolation operator I_n^{n+1} can be determined exactly using a space-time approach[23,24]; however, doing so in three dimensions poses a problem in four-dimensional mesh generation. Instead, an approximate scheme is desired that maintains conservation away from the region of the relative motion. The current scheme determines I_n^{n+1} exactly for all cells away from the moving boundary, as well as the majority of the cut cells at both time levels. For a small minority of the swept cells I_n^{n+1} is approximated.[16] In the current work, the mapping of the solution between two meshes is processed external to the flow solver with a single-pass algorithm. Note that because the motion is prescribed, all of the meshes can be processed a priori and in parallel.

An oscillating NACA 0012 airfoil is used to examine the behavior of the aforementioned approximate, relative-motion scheme. The oscillating airfoil has physical mechanisms similar to the dithering canards of the current missile configuration, and provides a well-documented test case. The transonic AGARD experiment[25] was computed using both the second-order backward scheme with the conservative, moving-domain ALE scheme and the first-order (in time) relative-motion scheme. Both schemes utilize the same spatially second-order numerical flux formulation. The computed normal force variations with angle of attack are shown in Fig. 5. Both simulations capture the hysteresis caused by the unsteady shock formation and are in relatively good agreement with the experimental data. Flow visualizations show no appreciable differences between the two simulations.

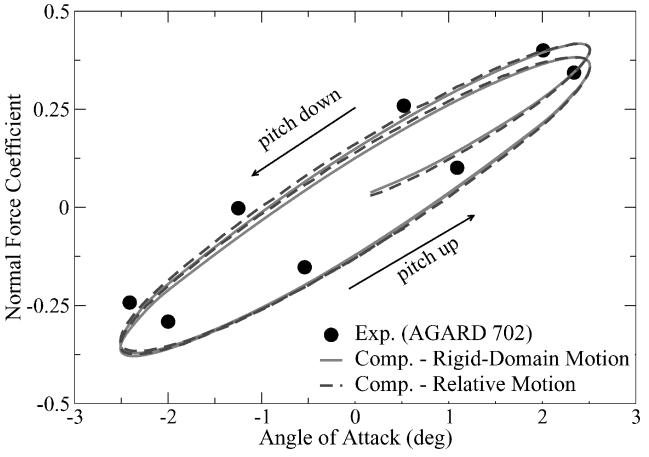

Fig. 5 Time history of normal force coefficient for an oscillating NACA 0012 airfoil. Experimental data from Ref. 25 [$M_\infty = 0.755$, $\alpha(t) = 0.016 + 2.51\sin(2\pi 62.5t)$].

III. Numerical Results

The general three-dimensional Cartesian scheme outlined earlier is utilized to simulate the rolling-missile geometry with movable canards described in Sec. II.A. These simulations are intended to both demonstrate the capabilities of the method and examine several topics pertinent to the current application. The dynamic effects are examined by comparison with a series of static, steady-state simulations. The suitability of the method as a predictive tool for rolling airframes is examined, and the computed results are compared against both viscous simulations and relevant experimental data. Comparisons with experimental data are included for both the rolling airframe with dithering canards and the prediction of dynamic stability derivatives.

A. Static-Roll Baselines

At the flow conditions of interest for the current work ($M_\infty = 1.6$, $\alpha = 3.0$ deg), with the body rolling at 8.75 Hz, a particle travels one body length in approximately 8 deg of revolution. (The nondimensional roll rate based on the freestream velocity and body diameter is $Sr_D = 0.0087$.) A particle in the canard vortex travels from the canard tip to the aft end of the body in approximately 6 deg of body roll. This relatively low roll rate (and corresponding low vortex twist) implies that a series of static computations at different roll and canard orientations should be a good approximation for the true dynamic behavior. A series of sequential-static simulations of the current rolling/dithering missile were performed in order to have a baseline for comparison with the dynamic simulations.

Static, steady-state simulations were performed at 2-deg increments of roll using both dither schedules 0 and 1 from Fig. 2 to schedule the canard pitch angle. The computed forces for both sequential-static series of computations are summarized in Fig. 6. The axial force for both dither schedules remains relatively constant

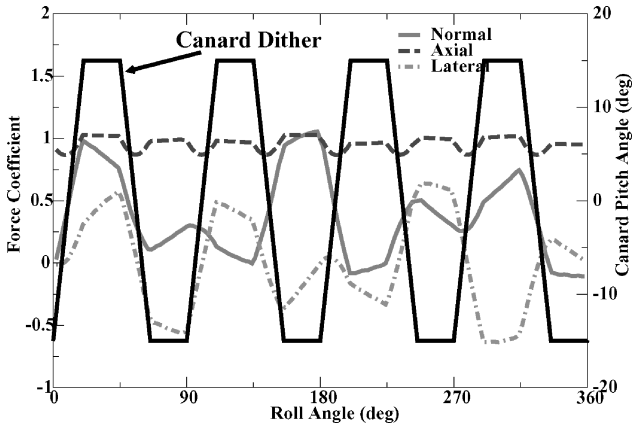

a) Dither schedule 0

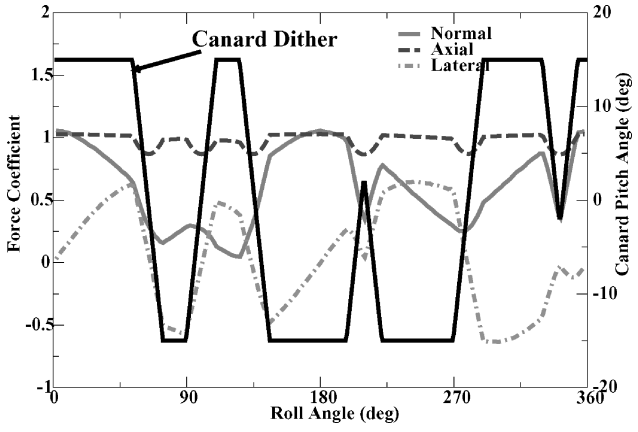

b) Dither schedule 1

Fig. 6 Computed force variation with roll angle for sequential-static simulations ($M_\infty = 1.6$, $\alpha = 3.0$ deg, $\dot{\phi} = 8.75$ Hz).

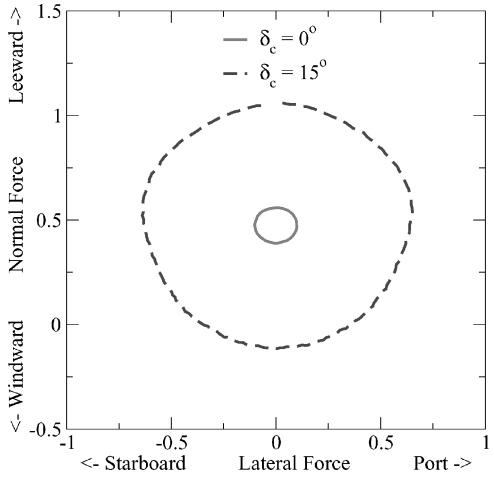

Fig. 7 Crossflow forces for sequential-static roll simulations with the canards held fixed and level ($M_\infty = 1.6$, $\alpha = 3.0$ deg, $\dot{\phi} = 8.75$ Hz).

and is effectively a function of the exposed frontal area of the canards. Both the lateral and normal forces show an immediate and strong response to changes in canard position. Note that in these static simulations a change in canard position is "felt" instantaneously by the tail section. In both dither schedules the normal and lateral forces change due to both roll orientation and canard pitch angle. For instance, in dither schedule 1 the normal force falls off while the lateral force increases as the body begins to roll. When the canards dither at $\phi = 55$ deg, it has only a moderate effect on normal force as the canards are approaching vertical; however, it causes the lateral force to immediately change sign. This is due to the canard lifting surfaces providing the majority of the lateral force in this roll orientation, because the canard vortices are located in a vertical plane. Similar analysis of the force response can be carried out for the entire roll/dither cycle.

While the details of the force and moment variations with roll angle provide insight, the main focus of the current work is to analyze the effect of the dynamics and canard dither on the roll-averaged loads. Figure 7 introduces a novel method for analyzing the roll behavior of the missile where the normal force and lateral force are simultaneously displayed in a crossflow plot as the body rolls. In Fig. 7 the canards are fixed throughout the roll cycle, and the crossflow forces inscribe a circular shape as the body rotates, as the canards continuously transition from providing normal force to lateral force and vice versa. A nearly identical plot can be generated by considering the pitching moment and yawing moment instead of normal and lateral forces. When the canards are held fixed and level ($\delta_c = 0.0$ deg) the crossflow force plot is circular. When the canards are fixed at their maximum deflection position ($\delta_c = 15.0$ deg), the shape slightly emphasizes the pitch-up plane, and the increase in available control power from the canards is evident as the radius of the "crossflow circle" has greatly expanded. Similarly, as the angle of attack increases the entire crossflow plot moves upward as more normal force is produced. Figure 8 presents a similar crossflow force plot with the canards now dithering. The dithering can be utilized to favor a particular region in the crossflow plane as the body rolls (relative to the circular plot for fixed canards). Dither schedule 0 provides less normal force (and pitch-up) than the fixed canard simulation, whereas dither schedule 1 provides an increase in normal force along with a slight roll-averaged lateral force. The bilateral symmetry of the plots is highlighted by including a solid line along the approximate axis of symmetry. The roll-averaged force lies on this axis of symmetry (see also Table 1). The crossflow forces follow the fixed-canard circular curve for portions of the arc, then cross to another section of the arc as the control signal moves the canards from maximum to minimum deflection while the body rolls.

B. Dynamic Computations with Dithering Canards

With the unconditionally stable implicit numerical scheme in the current work, the time step is limited by physical considerations

Table 1 Roll-averaged forces and moments for dither schedules 0 and 1[a]

Case	C_A	C_N	C_Y	C_l	C_m	C_n
Static, 8.75 Hz, schedule 0	0.95	0.37	0.0015	N/A	N/A	N/A
Dynamic, 8.75 Hz, schedule 0	0.95	0.38	−0.035	0.013	0.18	−0.011
Dynamic, 17.5 Hz, schedule 0	0.95	0.38	−0.035	−0.020	0.19	−0.25
Static, 8.75 Hz, schedule 1	0.97	0.62	0.049	N/A	N/A	N/A
Dynamic, 8.75 Hz, schedule 1	0.97	0.62	0.026	0.013	2.5	0.38

[a]The moment center is located a half body length from the nose ($M_\infty = 1.6$, $\alpha = 3.0$ deg).

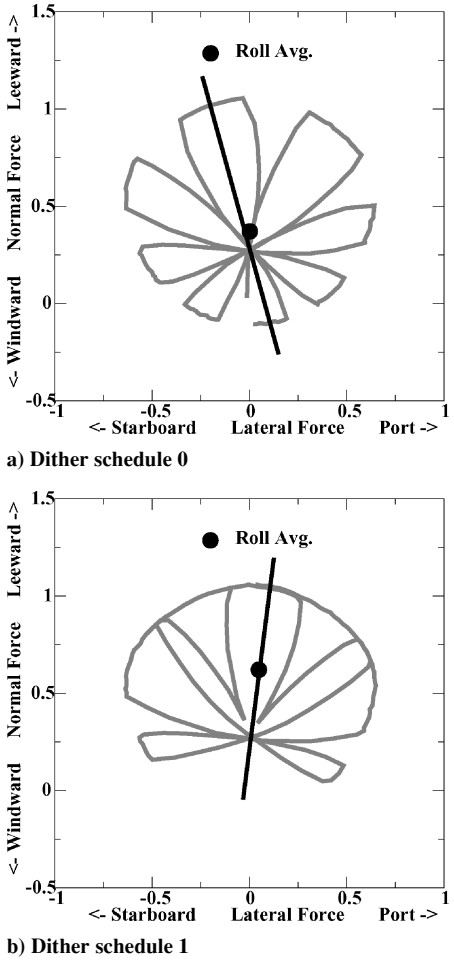

Fig. 8 Crossflow force for sequential-static roll simulations with canards dithering ($M_\infty = 1.6$, $\alpha = 3.0$ deg, $\dot{\phi} = 8.75$ Hz).

and accuracy rather than stability. An appropriate time step must be determined for each unsteady simulation, much as an appropriate mesh resolution must be chosen for static simulations. One method for determining a time step is to utilize a mesh that resolves all of the spatial scales of interest for the current problem, and perform a time-resolution study using this mesh. The 3.4M cell mesh from the mesh-resolution study described in Sec. II.A was utilized to compute a series of dynamic roll computations with the canards fixed at their maximum pitch angle ($\delta_c = 15.0$ deg). Three simulations with increasingly finer time resolutions were computed, along with a sequential-static simulation. The computed normal and lateral forces for this time-resolution study are presented in Fig. 9. All unsteady simulations were computed until the flowfield was periodic against the previous revolution of the body. Only results from the periodic portion of the time history (after the initial transients

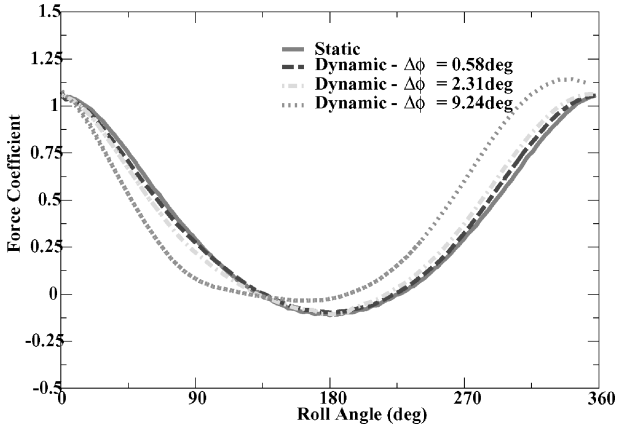

a) Normal force

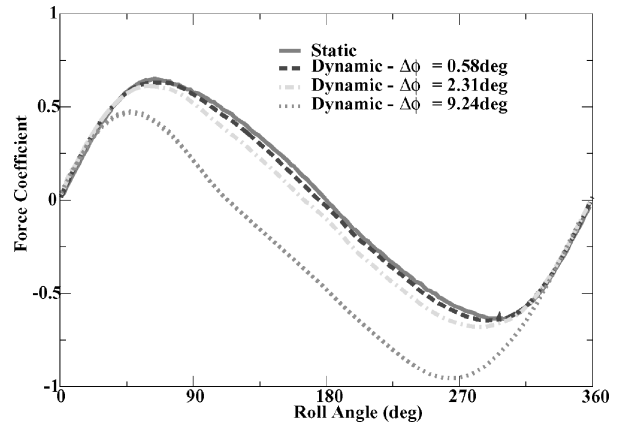

b) Lateral force

Fig. 9 Time-resolution study with fixed canards and constant roll rate ($M_\infty = 1.6$, $\alpha = 3.0$ deg, $\dot{\phi} = 8.75$ Hz, $\delta_c = 15.0$ deg).

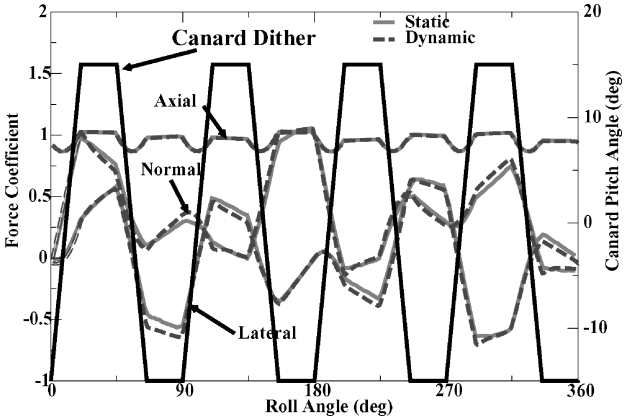

a) Dither schedule 0

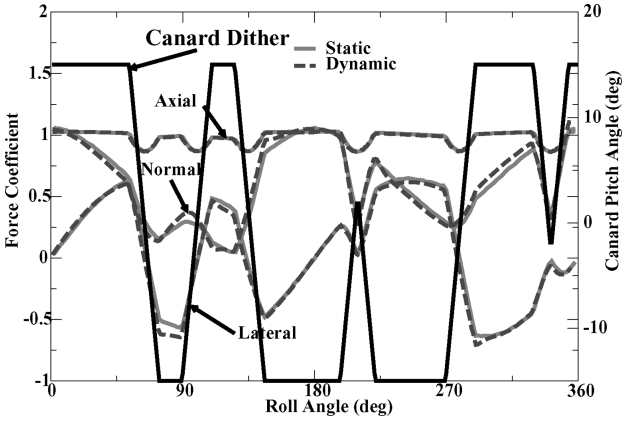

b) Dither schedule 1

Fig. 10 Comparison of static and dynamic force variation with roll angle with the canards dithering ($M_\infty = 1.6$, $\alpha = 3.0$ deg, $\dot{\phi} = 8.75$ Hz).

are removed) are presented. Because the canards are fixed, the force variation is sinusoidal and should maintain nearly the same peak values as the sequential-static simulations, with a roughly 6-deg lag due to the body rotation at this roll rate. It is seen that this is provided by the finest time step computed, $\Delta t = 0.58$ deg of roll. As a compromise between accuracy and computational cost, a time step of $\Delta t = 1.0$ deg of roll was utilized for all subsequent computations.

To examine the dynamic effects for the rolling airframe, the dither schedules presented in Fig. 2 were computed using the Cartesian general moving boundary scheme outlined in Sec. II.B. The force variation for both dither schedules is compared to the sequential-static simulations in Fig. 10. The agreement between the static and dynamic simulations is very close, as anticipated (the axial forces show no perceivable differences). Whenever the canards abruptly stop their motion, the fluid cannot respond instantaneously to the rigid structural motion and, hence, the dynamic simulations "overshoot" the static simulations. An example of this is seen near $\phi = 290$ deg for dither schedule 0. The dynamic simulation predicts slightly more normal force magnitude at the end of the canard dither motion and then underpredicts after the motion has stopped. This behavior is similar to the hysteresis seen in Fig. 5 for the oscillating airfoil. The predicted roll-averaged quantities are summarized in Table 1. There is close agreement between the static and dynamic roll-averaged normal and axial forces, and somewhat larger percentage differences in the lateral forces.

Figure 11 shows snapshots of velocity magnitude cutting planes (blue is low, red is high) from the dynamic simulation for dither schedule 0. These show that the canard vortices convect back to the exit plane of the computational domain aft of the tail fins. At this angle of attack, there is a strong interaction between the canard vortices and the tail fins. The canard tip vortex can be seen just outside the tail-fin bow shock in the last axial cutting plane on the body. The twist of the canard vortices is evident, though difficult to discern at this low body-roll rate. The change in the shock structure on the canards as they dither can be seen as well as the change in sense of rotation of the canard tip vortices.

Crossflow force comparisons of the static and dynamic simulations for both dither schedules are presented in Fig. 12. The effect of the dynamics can be seen as enlarging the areas of the "leaves" of the rosettes, as compared to the static simulations. The roll rate changes the sweep of the leaf, whereas the canard motion changes the outer limit.

As noted in the comparison of the static and dynamic simulations, the dynamic effects with the body rolling at 8.75 Hz are not substantial. To assess the dynamic effects at higher roll rates, a simulation was performed using a roll rate of 17.5 Hz and dither schedule 0. Note that, at this higher roll rate, the canards dither half as frequently than as shown in Fig. 2, which is limited by the mechanical response time of the canard actuator. The dither schedule for this higher roll rate is included in the summary force and moment plots in Fig. 13. It is shown that while the higher roll rate produces a different variation of the forces and moments with roll angle, the roll-averaged values are nearly unchanged (cf. Table 1). The roll-averaged rolling moment does decrease at the higher roll rate due to the cant of the tail fins. The yawing moment also increases in magnitude as the aft end of the body lags the canards at the higher roll rate. The effects of roll rate will be discussed further in the next section on dynamic derivatives. A comparison of the crossflow forces for the 8.75- and 17.5-Hz roll rates is presented in Fig. 14. The two paths are different, but both are similar to the fixed canard results of Fig. 7 and provide the same mean forces. The loss of canard control power is seen as the higher roll rate follows the fixed-canard curve for longer intervals.

A viscous, high-resolution (40M cells, 12,000 time steps/revolution) reference simulation by Nygaard and Meakin[13] is utilized as a baseline for comparison with the current inviscid results.

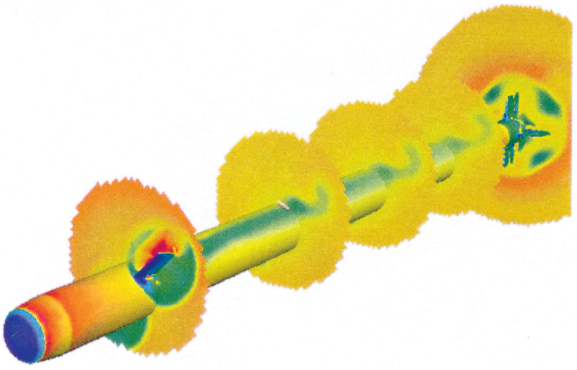

a) $\phi = 45.5$ deg

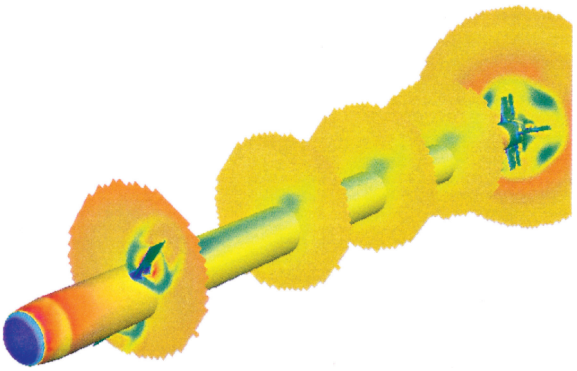

b) $\phi = 57.6$ deg

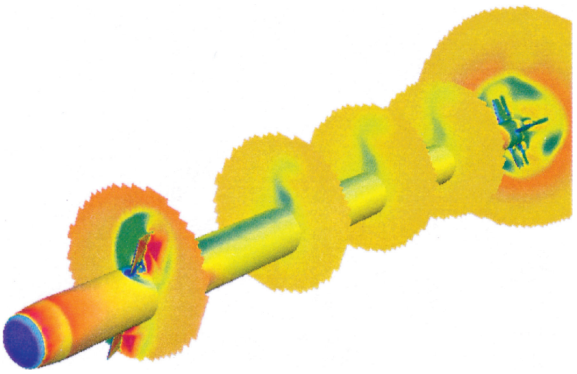

c) $\phi = 71.8$ deg

Fig. 11 Velocity magnitude contours from the dynamic computations for dither schedule 0 ($M_\infty = 1.6$, $\alpha = 3.0$ deg, $\dot{\phi} = 8.75$ Hz).

Table 2 Roll-averaged forces and moments for Fig. 16 dither schedule[a]

Values	C_N	C_Y	C_l	C_m	C_n
Experiment[14]	0.45–0.61	0.15–0.20	−0.036–0.019	−1.5–0.40	0.93–1.5
Computed	0.55	0.20	−0.034	−0.48	1.46

[a]The moment center is located a half body length from the nose ($M_\infty = 1.6$, $\alpha = 3.0$ deg, $\dot{\phi} = 18$ Hz).

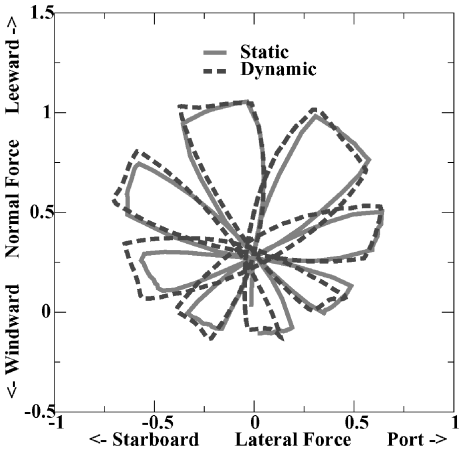

a) Dither schedule 0

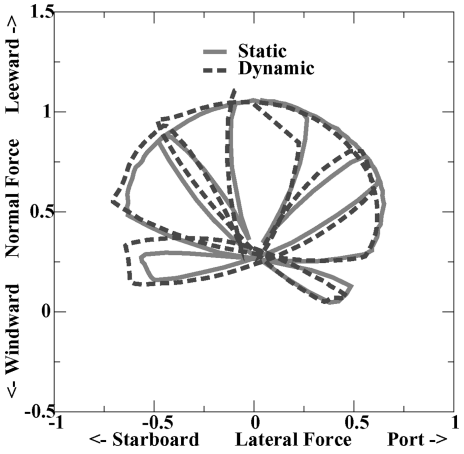

b) Dither schedule 1

Fig. 12 Comparison of static and dynamic crossflow forces with canards dithering ($M_\infty = 1.6$, $\alpha = 3.0$ deg, $\dot{\phi} = 8.75$ Hz).

The computed forces and moments for the simulation using dither schedule 0 are compared to the viscous simulations in Fig. 15. The agreement between the two simulations is very good throughout the roll cycle. As expected, there is a constant increment in axial force between the current inviscid results and the viscous simulations due to wall shear stress. The viscous results do consistently predict a slightly higher normal force through the roll cycle and a slightly lower (more nose down) pitching moment compared to the current results.

To assess the predictive capability of the current approach, a simulation of a recent experimental test[14] was performed. The experiment included both the ability to roll the airframe and dither the canards and also provided a measure of the experimental uncertainty. The actual canard motion from the experiment over 10 revolutions is presented in Fig. 16 along with an ensemble of averages of the canard position and an analytic approximation to the ensemble average, which is used to schedule the canards in the simulation. Again, the canard dither motion is periodic over a single body revolution. The computed forces and moments using this dither motion are presented in Fig. 17. The forces and moments again show an immediate and strong response to the motion of the canards. As opposed to the previous dither computations, this dither motion produces a yaw of the body. This can be clearly seen in the plot of crossflow forces (Fig. 18). The roll-averaged forces and moments are compared against the experimental values in Table 2. In all cases, the computed values are within the 95% confidence level for the experimental data.

C. Dynamic Derivatives with Fixed Canards

The preceding sections simulate the actual time-dependent motion of the rolling missile with dithering canards. Rather than simulate the actual motion for each dynamic case of interest, it is preferable in many cases to build a computational database that is capable of simulating any dynamic motion. One common method of building a computational database is to perform a parametric study for all of the possible geometric configurations and freestream conditions using a static, steady-state flow solver. This approach can be extended to include dynamic effects by performing a similar parametric study, varying the relevant dynamic parameters such as body roll rate.[9,26] From this dynamic parameter study, dynamic stability derivatives can be computed and used with the static derivatives to build a computational database. This approach is especially relevant to missile

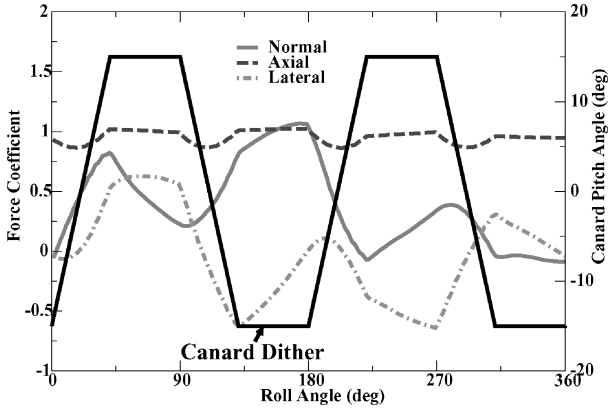

a) Forces

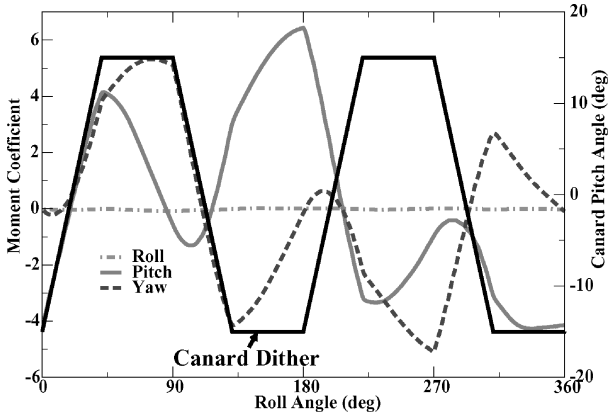

b) Moments

Fig. 13 Dynamic load variation at 17.5 Hz body roll rate ($M_\infty = 1.6$, $\alpha = 3.0$ deg, $\dot{\phi} = 17.5$ Hz).

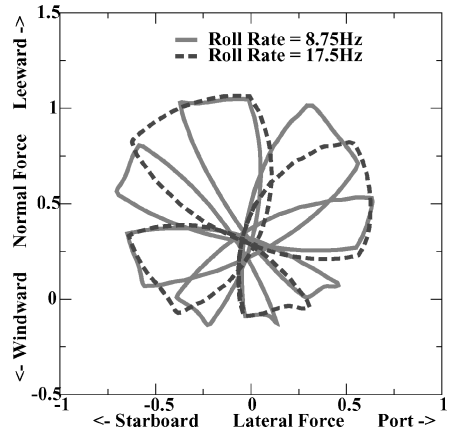

Fig. 14 Comparison of dynamic crossflow forces with dithering canards at different body roll rates ($M_\infty = 1.6$, $\alpha = 3.0$-deg.

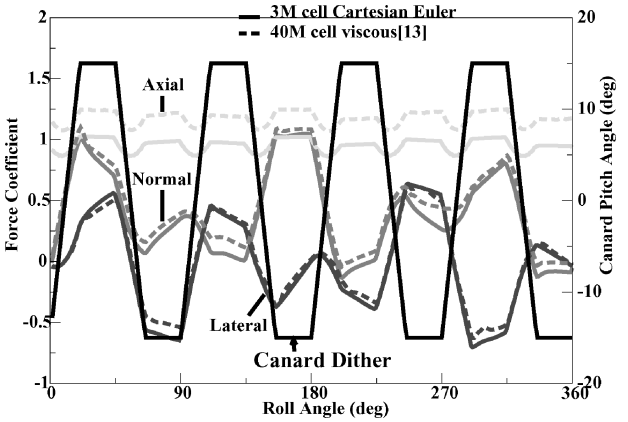

a) Forces

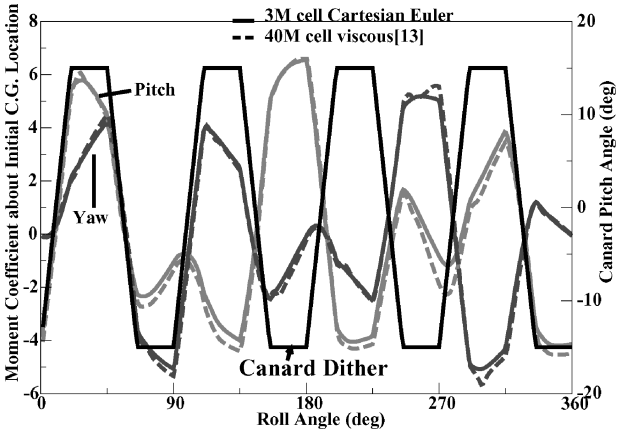

b) Moments

Fig. 15 Comparison of dither schedule 0 load histories with viscous results from Nygaard and Meakin[13] ($M_\infty = 1.6$, $\alpha = 3.0$ deg, $\dot{\phi} = 8.75$ Hz).

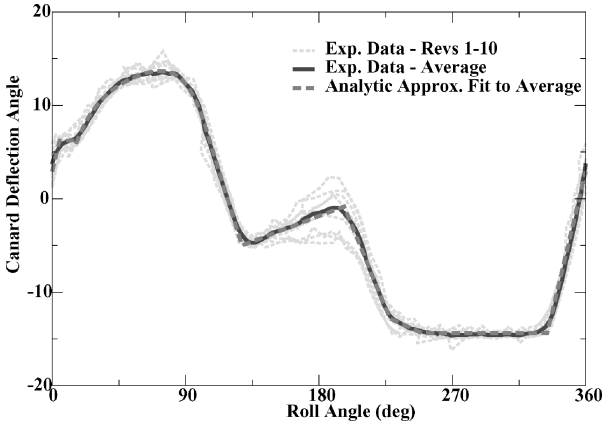

Fig. 16 Experimentally measured canard motion[14] ($M_\infty = 1.6$, $\alpha = 3.0$ deg, $\dot{\phi} = 18$ Hz).

configurations, which are highly maneuverable (e.g., $\pm 15g$) and, hence, frequently encounter an extreme range of flow conditions that require the higher-order dynamic derivatives.

The current work demonstrates a Cartesian method for calculating dynamic stability derivatives. The Cartesian scheme is advantageous for this application because the process can be completely automated. Further, the ALE formulation outlined in Sec. II.B.2 can be utilized when there is no relative motion present, leading to an efficient scheme for dynamic computations. Simulations of the rolling missile with the canards fixed in the zero-deflection position were performed at three roll rates to match the available experimental data[14]: 9, 12, and 18 Hz. For the current configuration, the quantities of primary interest for dynamic modeling are the roll and yaw derivatives:

$$C_{l_p} = \frac{2V_\infty}{D}\frac{\partial C_l}{\partial p}, \qquad C_{n_p} = \frac{2V_\infty}{D}\frac{\partial C_n}{\partial p} \tag{7}$$

where p is the roll rate. All quantities that affect the integrated loads besides roll rate, such as angle of attack or freestream Mach number, are held constant while taking the derivative in Eq. (7). The variation of pitching moment was also calculated; however, the pitching moment remains essentially constant at the roll rates and angle of attack being investigated here. Figure 19 presents the variation of the yaw and roll moments against the experimental data. The agreement with the experimental data is very good, and all of

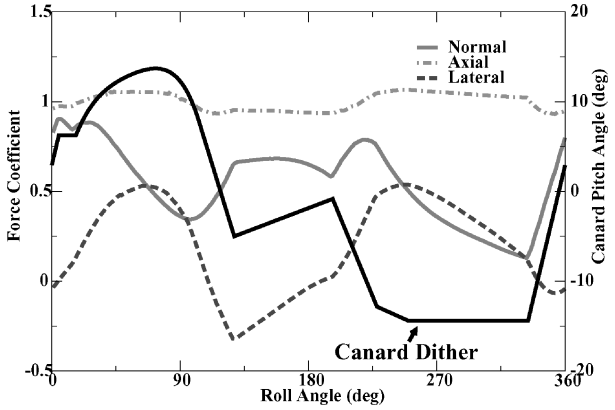

a) Forces

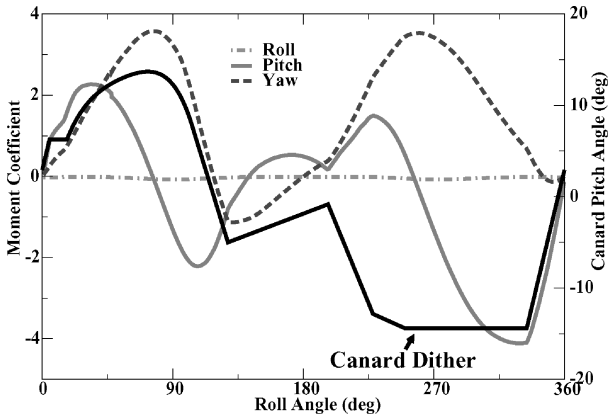

b) Moments

Fig. 17 Dynamic load variation for Fig. 16 dither schedule ($M_\infty = 1.6$, $\alpha = 3.0$ deg, $\dot{\phi} = 18.0$ Hz).

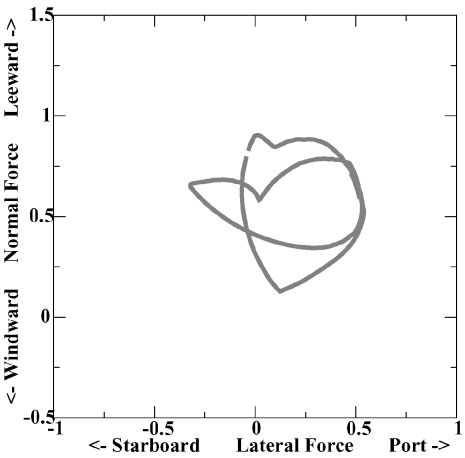

Fig. 18 Dynamic crossflow forces for Fig. 16 dither schedule ($M_\infty = 1.6$, $\alpha = 3.0$ deg, $\dot{\phi} = 18.0$ Hz).

the computed data points are within the experimental uncertainty. At these relatively low roll rates, both the yawing and rolling moments show a linear dependence on roll rate. Hence, the damping coefficients correspond to the slopes of the curves in Fig. 19. As the roll rate is increased, the canard vortices experience more twist as they travel the length of the body. This increase in twist causes the yawing moment relative to the c.g. location to increase as the roll rate increases and as the flow on the aft end increasingly lags behind the canards. The rolling moment is most strongly influenced by the cant of the tail fins. At these flow conditions, both the computations and experiment show that if the missile were unconstrained, the fins would cause it to roll at 10–15 Hz.

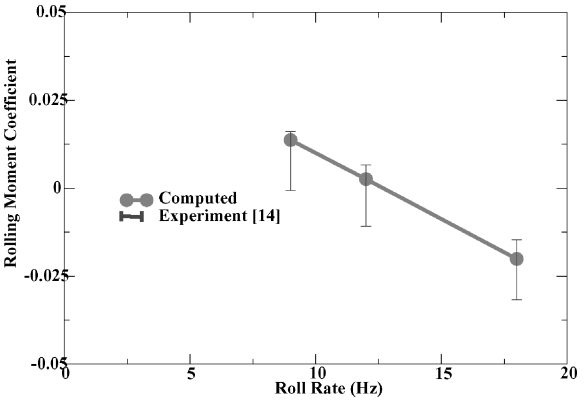

a) Roll

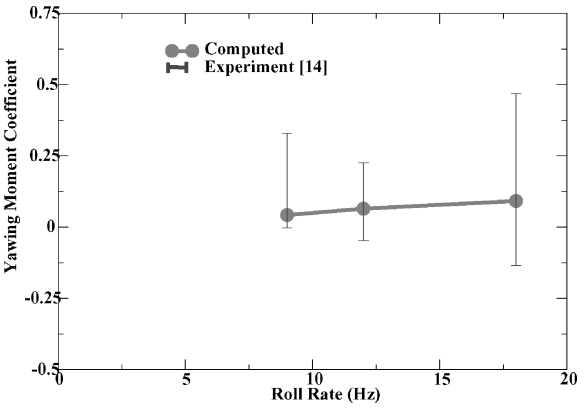

b) Yaw

Fig. 19 Dynamic derivatives with fixed canards ($M_\infty = 1.6$, $\alpha = 3.0$ deg, $\delta_c = 0.0$ deg).

IV. Summary

A three-dimensional Cartesian method for simulating the general prescribed motion of rigid bodies was developed and applied to the analysis of a rolling airframe with movable canard control surfaces. The use of a Cartesian method enables dynamic simulations to be processed in a robust and automated manner. Dynamic simulations for several canard dither schedules and roll rates were performed and compared against static simulations, high-resolution viscous simulations, and relevant experimental data. The results show that the current scheme can be used as an effective predictive tool for both the complete rolling motion with canard dither as well as for computing dynamic stability derivatives. At the relatively low roll rates considered in this work, a series of static, steady-state simulations provides a good approximation to the actual dynamic motion. Comparisons with the viscous results of Nygaard and Meakin[13] show that the current inviscid results capture the same trends and can be corrected with a constant viscous axial force increment. Direct comparison with recent experimental data shows that the computed forces and moments are within the experimental uncertainty for all simulations considered.

Acknowledgments

Marsha Berger was supported by AFOSR Grant F19620-00-0099 and DOE Grants DE-FG02-00ER25053 and DE-FC02-01ER25472. The authors thank Tor Nygaard of ELORET and Robert Meakin of the U.S. Army Aeroflight Dynamics Directorate for providing the viscous simulation results for comparison. The analytic canard dither model was developed by John Stalnaker of SYColeman.

References

[1]Aftosmis, M. J., Berger, M. J., and Melton, J. E., "Robust and Efficient Cartesian Mesh Generation for Component-Based Geometry," *AIAA Journal*, Vol. 36, No. 6, 1998, pp. 952–960.

[2]Aftosmis, M. J., Berger, M. J., and Adomavicius, G., "A Parallel Multilevel Method for Adaptively Refined Cartesian Grids with Embedded Boundaries," AIAA Paper 2000-0808, Jan. 2000.
[3]Meakin, R. L., and Suhs, N., "Unsteady Aerodynamic Simulation of Multiple Bodies in Relative Motion," AIAA Paper 89-1996, June 1989.
[4]Batina, J., "Unsteady Euler Algorithm with Unstructured Dynamic Mesh for Complex Aircraft Aeroelastic Analysis," AIAA Paper 89-1189, June 1989.
[5]Löhner, R., "Adaptive Remeshing for Transient Problems," *Computer Methods in Applied Mechanics and Engineering*, Vol. 75, 1989, pp. 195–214.
[6]Venkatakrishnan, V., and Mavriplis, D. J., "Computation of Unsteady Flows over Complex Geometries in Relative Motion," *Proceedings of 1st AFOSR Conference on Dynamic Motion CFD*, edited by L. Sakell and D. Knight, Rutgers Univ., 1996.
[7]Weinacht, P., Sturek, W. B., and Schiff, L. B., "Navier–Stokes Predictions of Pitch-Damping for Axisymmetric Shell Using Steady Coning Motion," AIAA Paper 91-2855, Aug. 1991.
[8]Weinacht, P., "Navier–Stokes Predictions of the Individual Components of the Pitch-Damping Sum," *Journal of Spacecraft and Rockets*, Vol. 35, No. 5, 1998, pp. 598–605.
[9]Oktay, E., and Akay, H. U., "CFD Predicitions of Dynamic Derivatives for Missiles," AIAA Paper 2002-0276, Jan. 2002.
[10]Park, S. H., Kim, Y., and Kwon, J. H., "Predicition of Dynamic Damping Coefficients Using Unsteady Dual-Time Stepping Method," AIAA Paper 2002-0715, Jan. 2002.
[11]Janus, J. M., Whitfield, D. L., Horstman, H. Z., and Mansfield, F., "Computation of the Unsteady Flowfield About a Counterrotating Prop-Fan Cruise Missile," AIAA Paper 90-3093, Aug. 1990.
[12]Hall, L. H., "Rolling Airframe Missile Aerodynamic Predictions Using a Chimera Approach for Dithering Canards," AIAA Paper 2002-0405, Jan. 2002.
[13]Nygaard, T., and Meakin, R., "An Aerodynamic Analysis of a Spinning Missile with Dithering Canards," AIAA Paper 2002-2799, June 2002.
[14]"Defensive Missile Wind Tunnel Test for the Validation and Verification of CFD Codes," Dynetics Technical Rept., Jan. 2002.
[15]Aftosmis, M. J., "Solution Adaptive Cartesian Grid Methods for Aerodynamic Flows with Complex Geometries," von Kármán Inst. Lecture Series 97-02, March 1997, pp. 1–105.
[16]Murman, S. M., Aftosmis, M. J., and Berger, M. J., "Implicit Approaches for Moving Boundaries in a 3-D Cartesian Method," AIAA Paper 2003-1119, Jan. 2003.
[17]Merkle, C. L., and Athavale, M., "A Time Accurate Unsteady Incompressible Algorithm Based on Artificial Compressibility," AIAA Paper 87-1137, June 1987.
[18]Rogers, S. E., Kwak, D., and Kiris, C., "Numerical Solution of the Incompressible Navier–Stokes Equations for Steady and Time-Dependent Problems," *AIAA Journal*, Vol. 29, No. 4, 1991, pp. 603–610.
[19]Jameson, A., "Time Dependent Calculations Using Multigrid with Applications to Unsteady Flows Past Airfoils," AIAA Paper 91-1596, June 1991.
[20]Melson, N. D., Sanetrik, M. D., and Atkins, H. L., "Time-Accurate Navier–Stokes Calculations with Multigrid Acceleration," *Proceedings of the Sixth Copper Mountain Conference on Multigrid Methods*, April 1993.
[21]Hirt, C. W., Amsden, A. A., and Cook, J. L., "An Arbitrary Lagrangian-Eulerian Computing Method for All Flow Speeds," *Journal of Computational Physics*, Vol. 14, 1974, pp. 227–253.
[22]van Leer, B., "Flux-Vector Splitting for the Euler Equations," *Lecture Notes in Physics*, Vol. 170, Springer-Verlag, Berlin, 1982, pp. 507–512.
[23]Zhang, H., Reggio, M., Trépanier, J. Y., and Camarero, R., "Discrete Form of the GCL for Moving Meshes and its Implementation in CFD Schemes," *Computers in Fluids*, Vol. 22, No. 1, 1993, pp. 9–23.
[24]Lesoinne, M., and Farhat, C., "Geometric Conservation Laws for Flow Problems with Moving Boundaries and Deformable Meshes, and Their Impact on Aeroelastic Computations," *Computer Methods in Applied Mechanics and Engineering*, Vol. 134, 1996, pp. 71–90.
[25]Landon, R. H., "Compendium of Unsteady Aerodynamic Measurements," AGARD Rept. 702, Aug. 1982.
[26]Park, M. A., and Green, L. L., "Steady-State Computation of Constant Rotational Rate Dynamic Stability Derivatives," AIAA Paper 2000-4321, June 2000.

P. Weinacht
Associate Editor